atmosphere

MDPI

Article

Meteorological and Hydrological Drought Risks under Future Climate and Land-Use-Change Scenarios in the Yellow River Basin

Yunyun Li [1,*], Yi Huang [1], Jingjing Fan [2], Hongxue Zhang [3,*], Yanchun Li [1], Xuemei Wang [1] and Qian Deng [1]

[1] Ecological Security and Protection Key Laboratory of Sichuan Province, Mianyang Normal University, Mianyang 621000, China; 13018241926@163.com (Y.H.); 13440169382@163.com (Y.L.); wangxuemei13@mails.ucas.ac.cn (X.W.); 13548492076@163.com (Q.D.)
[2] College of Water Resources and Hydropower, Hebei University of Engineering, Handan 056038, China; fanjingjing@hebeu.edu.cn
[3] College of Water Conservancy & Civil Engineering, Northeast Agricultural University, Harbin 150030, China
* Correspondence: liyunyun@mtc.edu.cn (Y.L.); hongxue@neau.edu.cn (H.Z.)

Abstract: The primary innovation of this study lies in the development of an integrated modeling framework that combines downscaled climate projections, land-use-change simulations, and copula-based risk analysis. This framework allows for the assessment of localized sub-seasonal and seasonal drought hazards under future scenarios. The BCC-CSM1-1 climate model projections from the NASA Earth Exchange Global Daily Downscaled Projections (NEX-GDDP) dataset are utilized to represent the future climate for 2025–2060 under RCP 4.5 and 8.5 scenarios. The CA-Markov model is employed to predict future land-use-change distributions. The climate–land use–drought modeling nexus enables the generation of refined spatio-temporal projections of meteorological and hydrological drought risks in the Yellow River Basin (YRB) in the future period of 2025–2060. The results highlight the increased vulnerability of the upper YRB to sub-seasonal meteorological droughts, as well as the heightened sub-seasonal hydrological drought risks in the Loess Plateau. Furthermore, downstream areas experience escalated seasonal hydrological drought exposure due to urbanization. By providing actionable insights into localized future drought patterns, this integrated assessment approach advances preparedness and climate adaptation strategies. The findings of the study enhance our understanding of potential changes in this integral system under the combined pressures of global climate change and land use shifts.

Keywords: meteorological drought; hydrological drought; drought risk prediction; future climate and land-use-change scenarios

Citation: Li, Y.; Huang, Y.; Fan, J.; Zhang, H.; Li, Y.; Wang, X.; Deng, Q. Meteorological and Hydrological Drought Risks under Future Climate and Land-Use-Change Scenarios in the Yellow River Basin. *Atmosphere* **2023**, *14*, 1599. https://doi.org/10.3390/atmos14111599

Academic Editors: Pengcheng Yan, Ognjen Bonacci and Luis Gimeno

Received: 10 September 2023
Revised: 19 October 2023
Accepted: 23 October 2023
Published: 26 October 2023

1. Introduction

In recent decades, meteorological and hydrological events at a regional and global scales have imparted substantial impacts on agricultural, ecological, and public water systems. Despite rapid advancements in science and technology, the ramifications of such droughts remain profound. For example, approximately 12 billion km^2 of cropland were affected and over 10 million fatalities incurred due to droughts worldwide between 1900 and 2010 [1,2]. More recently, major meteorological and hydrological drought episodes, including the 2011 East Africa drought, 2012 U.S. Central Great Plains drought, and 2012–2015 California drought, have garnered significant attention due to their extensive agricultural and societal impacts [3–7]. China has also historically experienced frequent meteorological and hydrological drought incidences historically, especially in the ecologically fragile and geographically complex Yellow River Basin (YRB), profoundly influencing agricultural, economic and social development. Numerous scholarly works have examined drought patterns within the YRB region [8–11]. For instance, Zhu et al. [12] assessed integrated

drought conditions in the YRB utilizing a comprehensive drought index, ascertaining a drying trend inclination over recent decades, with heightened aridity in upstream and northern sections. Li et al. [13] evaluated the hydrological drought evolution using a non-linear joint index, identifying increasingly severe hydrological droughts in recent decades, particularly across the Loess Plateau. Wang et al. [14] inspected the interrelationships between hydrological and meteorological droughts in the YRB, reiterating exacerbated hydrological drought patterns. Collectively, these investigations accentuate the substantial impacts of meteorological and hydrological droughts across the ecologically and socially vital YRB territory.

Against the backdrop of global change, the YRB, which is ecologically significant, may experience shifts in meteorological and hydrological drought patterns. Several studies have sought to understand potential variations in drought characteristics in the YRB under climate change projections. For instance, Ji et al. [15] assessed the spatiotemporal patterns of future meteorological drought in the YRB under different representative concentration pathway (RCP) scenarios. Wang et al. [16] analyzed the characteristics of meteorological drought in the YRB using SPEI indicators and projections from five Global Climate Models (GCMs) under three scenarios of the Shared Socioeconomic Pathways (SSP) released in the Sixth Coupled Model Inter-comparison Project (CMIP6). Zhang et al. [17] investigated the hydrological drought variations in the upper Yellow River Basin (UYRB) during 2021–2100, employing the latest Coupled Model Inter-comparison Project Phase 6 (CMIP6) datasets. Generally, while prior studies have evaluated future meteorological and hydrological drought characteristics in the ecologically vital YRB resulting from climate change, research gaps remain in assessing drought risks under concurrent climate and land use changes. Global change involves not just climate variations but also land use alterations from human activities like agricultural expansion, afforestation, and urbanization. Land use changes can modify regional hydrological cycles and linkages between meteorological and hydrological droughts, indirectly exacerbating or relieving drought impacts [18]. Therefore, it is crucial to consider both climate change and shifts in land use patterns when projecting future hydrological drought risks.

Among the numerous studies on drought risk assessments, the copula function is a popular method widely used in drought risk analysis due to its flexibility and lack of dependence on marginal distributions [19–23]. Dai et al. [24] assessed agricultural drought risk and its dynamic evolution using copula functions in the Pearl River Basin. Yu et al. [25] performed copula-based drought frequency analysis using an aggregate drought vulnerability index within the Chungcheong province, South Korea. Chang et al. [26] assessed the multivariate integrated drought risk in the Wei River Basin through the joint probability distribution of drought duration and severity based on Archimedean copulas. Shaw and Chithra [27] developed a copula-based framework to investigate the meteorological and hydrological droughts using a multivariate analysis of drought characteristics in the Pennar River basin (a semi-arid region) of India. However, existing drought risk assessments using copula functions primarily focus on historical frequencies rather than future projections, leaving a gap in copula-based drought modeling under climate and land-use-change scenarios for the YRB.

To address these gaps, this research introduces an innovative integrated modeling framework that couples downscaled climate projections, land-use-change simulations, and copula-based risk analysis to evaluate localized sub-seasonal and seasonal drought hazards under future scenarios. The key innovation lies in the novel linkage of advanced climate, land use, and drought risk models, enabling a comprehensive methodology for evaluating sub-seasonal to seasonal drought risks under climate and land use change. Examining meteorological and hydrological drought projections for the YRB will provide greater understanding of potential changes to this integral system under global change pressures from climate and land use shifts.

The three primary objectives are (1) to simulate and analyze projected land use changes across the YRB, (2) to construct a copula-based drought risk model using joint probability

distribution of duration and severity, and (3) to apply the integrated model to predict sub-seasonal and seasonal meteorological and hydrological drought risks and interconnections under future climate and land use changes.

2. Study Area and Data Sources

2.1. The Yellow River Basin

The Yellow River Basin (YRB) holds a significant position as the second largest river basin in China and the sixth largest globally. It has played a crucial role in the development of Chinese civilization, providing water resources for approximately 140 million people and irrigating 15% of China's agricultural land. The YRB spans nine provinces, encompassing the Tibetan Plateau, Loess Plateau, and North China Plain before reaching the Bohai Sea. This expansive region exhibits substantial spatial variability in terms of elevation, precipitation, and temperature. The mean annual precipitation ranges from 123 mm to 1021 mm, gradually increasing from northwest to southeast. Simultaneously, the mean annual temperatures vary from −4 °C to 14 °C, influenced by both latitude and elevation [8].

To facilitate the systematic prediction of meteorological and hydrological drought risks across this heterogeneous and climatically diverse basin, the YRB has been divided into six subzones based on distinct climatic and topographic characteristics (Figure 1). Detailed descriptions of each subzone are available in the paper of Li et al. [13]. This zonal delineation will enable the spatial analysis of meteorological and hydrological drought hazards across the YRB, taking into account its diverse climatic and geographical features.

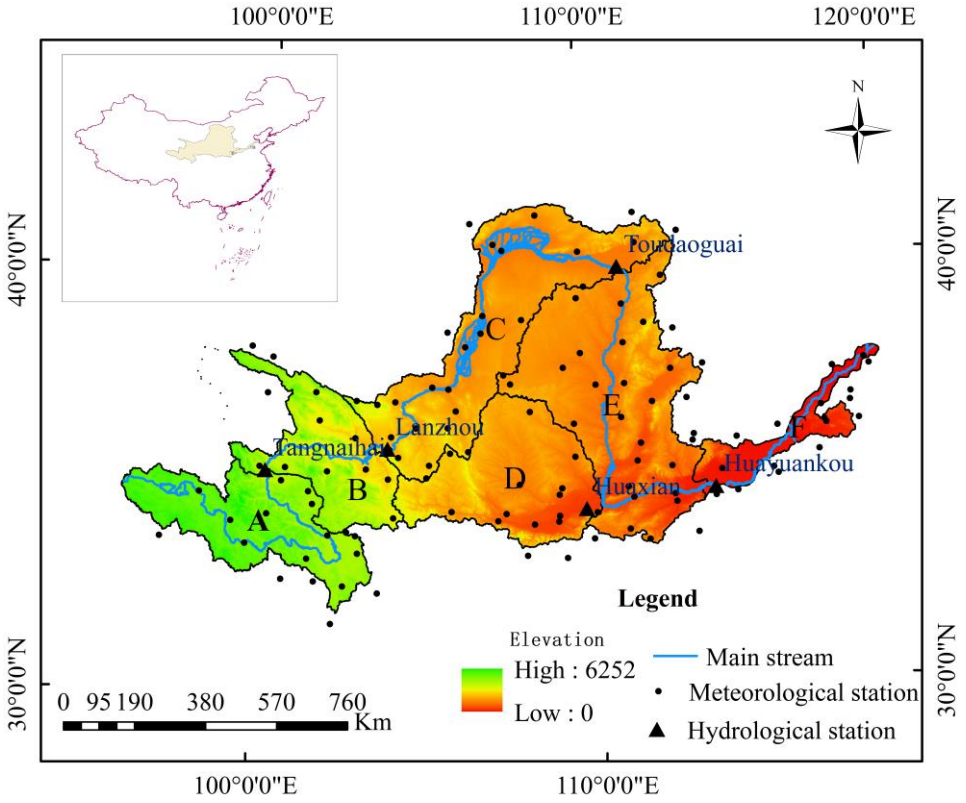

Figure 1. Map depicting the location and topography of the YRB and its six delineated zones. Zone A encompasses a semi-arid to semi-humid region with plateau climatic characteristics. Zone B represents a transitional zone between plateau and mid-temperate climates. Zone C comprises an arid to semi-arid region with mid-temperature climatic features. Zone D constitutes a semi-arid region with warm temperature climate traits. Zone E encompasses a semi-arid to semi-humid zone with a temperate continental climate. Zone F constitutes a humid region with temperate monsoonal climate characteristics.

2.2. Data Sources

2.2.1. NEX-GDDP Data

Projections of future climate under varying emissions scenarios are valuable for assessing meteorological and hydrological drought hazards. The National Aeronautics and Space Administration Earth Exchange Global Daily Downscaled Projections (NEX-GDDP) dataset provides statistically downscaled climate projections at high temporal (daily) and spatial ($0.25^\circ \times 0.25^\circ$) resolutions [28,29] (https://cds.nccs.nasa.gov/nex-gddp/ (accessed on 25 February 2021)). Compared to traditional general circulation models (GCMs), the NEX-GDDP increases spatial resolution and enhances the simulation of extreme climate values in the historical period, especially for topographically complex regions. This improves the accuracy of future climate change projections [30]. Several studies utilizing NEX-GDDP for meteorological drought analyses demonstrate its promise as a source of localized and regional-scale climate projections [31,32]. Therefore, this study employs the NEX-GDDP dataset to represent future climate conditions for assessing meteorological drought risk, as well as providing meteorological inputs for evaluating hydrological drought risk. The high-resolution NEX-GDDP data enable the robust examination of potential future drought hazards in the topographically and climatically diverse YRB.

Given the robust predictive capacity and skillful simulation demonstrated by the BCC-CSM1-1 model within the NEX-GDDP dataset for China's climate conditions [33], it was selected to provide downscaled projections for the period 2025–2060 under two Representative Concentration Pathway (RCP) scenarios (RCP4.5 and RCP8.5). These projections were utilized to evaluate the risks of meteorological and hydrological drought across the Yangtze River Basin (YRB), as the model accurately simulates the climate characteristics of this region, as detailed in Appendix A.

2.2.2. Observation Data

Meteorological data from 1970–2015, including daily maximum and minimum temperature, precipitation, humidity, solar radiation, and wind speed records from 121 weather stations (Figure 1), were obtained from the National Climate Center of China (http://data.cma.cn/ (accessed on 16 March 2021)). To calibrate and validate the SWAT model, naturalized monthly streamflow data from 1970–2015 at five hydrological stations (Figure 1) were acquired from the Yellow River Conservancy Commission. Naturalized streamflow refers to flow that excludes direct anthropogenic influences, such as reservoir storage, irrigation, and industrial, domestic and agricultural water withdrawals [13]. These high-resolution meteorological and hydrological records enable the robust calibration and validation of the SWAT model prior to simulating future hydrological conditions across the climatically and topographically diverse YRB.

2.2.3. Remote Sensing Monitoring Data

The spatial data utilized in this study included a digital elevation model (DEM), a digital stream network, a soil map, and four land-use maps. The 30 m resolution DEM data were extracted from the National Aeronautics and Space Administration's Shuttle Radar Topography Mission (SRTM) Digital Elevation Model (https://www.resdc.cn/ (accessed on 16 March 2021)). The 1:1,000,000 scale soil map and land-use maps for 1980, 1990, 2000, 2010 and 2020 were acquired from the Data Center for Resources and Environmental Sciences, Chinese Academy of Sciences (https://www.resdc.cn/ (accessed on 16 March 2021)). This high-resolution spatial data enable the accurate characterization of the topographically and environmentally diverse YRB, facilitating the hydrological modeling and analysis of land use changes.

3. Methodology

The detailed methodology is provided in this section, which mainly includes the SWAT model, future climate and land-use-change prediction, and the copula-based drought risk-assessment model. The flow chart of research is provided in Figure 2.

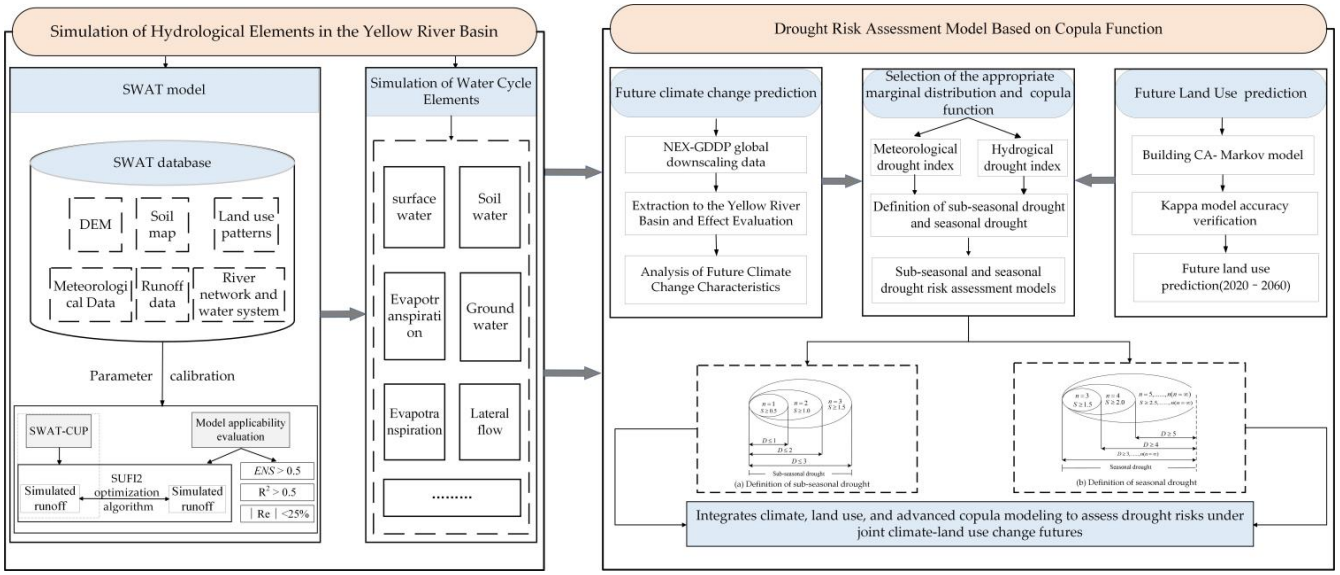

Figure 2. Flow chart of research.

3.1. Meteorological and Hydrological Drought Indices

The accurate selection or development of appropriate meteorological and hydrological drought indices is critical for effectively predicting associated risks. Numerous indices have been proposed for characterizing both meteorological and hydrological droughts [13,34,35]. Meteorological drought indices primarily encompass the Standardized Precipitation Index (SPI) [36], Precipitation Anomaly Percentage (PAP) [26], Standardized Precipitation Evapotranspiration Index (SPEI) [37], and Reconnaissance Drought Index (RDI) [38]. The SPEI and RDI are particularly well-suited for capturing meteorological drought, as they take into account both precipitation and evapotranspiration, which are direct drivers of drought [39]. Compared to the SPEI, the RDI exhibits greater sensitivity to environmental changes and provides clearer evaluation criteria by fitting a distribution function to the precipitation-potential evapotranspiration ratio [40]. Therefore, this study employed the RDI as the meteorological drought index. The detailed RDI calculation procedures can be found in the study of Tsakiris and Vangelis [41], along with the corresponding classification shown in Table 1.

Table 1. The classification of RDI.

RDI	Drought Grade
$RDI > -0.5$	No drought
$-1.0 < RDI \leq -0.5$	Abnormally dry
$-1.5 < RDI \leq -1.0$	Moderate drought
$-2.0 < RDI \leq -1.5$	Severe drought
$RDI \leq -2.0$	Extreme drought

In recent decades, several standardized indices have been developed to characterize hydrological drought. These indices include the Surface Water Supply Index (SWSI) [42], Palmer Hydrological Drought Severity Index (PHDI) [43], Standardized Runoff Index (SRI) [44], and Standardized Streamflow Index (SSI) [45]. However, these indices primarily focus on surface runoff or streamflow and do not adequately consider the groundwater component. Groundwater, which includes both recharge and discharge, plays a significant role in hydrological processes and has a substantial impact on hydrological drought [46–48]. Therefore, this study employs the Nonlinear Joint Hydrological Drought Index (NJHDI), proposed in our previous study by Li et al. [13], to effectively characterize hydrological drought. The NJHDI comprehensively considers surface water, groundwater, and their

nonlinear interconnections. The detailed procedures and classification criteria for the NJHDI can be found in the study of Li et al. [13]. The classification of the NJHDI aligns with that of the RDI, as presented in Table 1.

3.2. Land-Use-Change Prediction Model

3.2.1. CA-Markov Model

The Markov chain-cellular automata (CA-Markov) model is an effective and reliable method for the analysis and prediction of land use change across various time scales. This model combines the temporal Markov method with spatial cellular automata techniques [49,50]. The Markov chain is a stochastic modeling method based on the assumption that a system's state probability at a given time can be determined from its earlier state [51]. It has been widely applied to study land-use-change dynamics, accurately predicting the magnitude of change at broad scales, but lacks spatial distribution capabilities as spatial categories are not considered [52]. On the other hand, the cellular automata (CA) model incorporates spatial attributes by permitting computational experiments on spatial arrangements over time [53]. The integration of CA with Markov modeling has become a dominant technique for the assessment and prediction of land use change [54–58].

Therefore, this study employed the CA-Markov model to predict future spatial–temporal land use patterns based on historical trends. The CA-Markov module in IDRISI Andes v17.0 [55] was utilized, following five key steps: (1) calculation of the land-use-transition probability matrix through the spatial overlay of historical land-use maps; (2) determination of CA transition rules that describe changes in cell states; (3) generation of suitability maps that define the transition potential; (4) selection of 5×5 CA filters to define neighborhood cells; and (5) prediction of land-use maps for target years based on transition matrix and suitability maps. Further CA-Markov details are available in [54]. This approach coupled Markovian temporal modeling with spatial CA techniques to robustly project land-use-change trends.

3.2.2. Accuracy Assessment

In this study, the Kappa statistic was utilized to assess the accuracy and validity of the CA-Markov model. The Kappa statistic serves as a reliable metric for evaluating the agreements in the spatial patterns between two maps [56]. The calculation of *Kappa* is performed as follows:

$$Kappa = \frac{P_o - P_c}{1 - P_c} \quad (1)$$

where P_o represents the proportion of units that agree, while P_c represents the proportion of units in agreement with the expected change. If the value of *Kappa* falls between 0 and 0.4, it indicates a low level of agreement between the two maps. Conversely, if *Kappa* ranges from 0.4 to 0.7, it signifies a moderate level of agreement. Finally, if *Kappa* surpasses 0.7, it suggests a high level of agreement between the two maps.

3.3. SWAT Model

The Soil and Water Assessment Tool (SWAT) is a physical-based distributed hydrological model that operates in continuous time. It is capable of effectively representing the intricate hydrological processes occurring in watersheds with varying meteorological, land-use, soil, and geographical conditions, at different temporal scales (daily, monthly, and yearly) [59,60]. Therefore, in this study, the SWAT model was employed to simulate the hydrological processes influenced by climate and land use changes.

The performance of the SWAT model is assessed using three metrics: the Nash-Sutcliffe coefficient (*Ens*) [61], coefficient of determination (R^2), and percentage bias (PBIAS) [62]. According to Moriasi et al. [63], satisfactory performance of the SWAT model at the monthly scale is indicated by $Ens > 0.5$, $R^2 > 0.6$, and $|PBIAS| < 25\%$.

3.4. Definition of Drought Event and Characteristics

The occurrence of a drought event is primarily characterized by drought onset, drought duration, drought severity, and drought termination. Among these indicators, drought duration and drought severity are considered key factors in defining a drought event [26]. In this study, the runs theory [64] is utilized to identify a drought event and determine its duration (*D*) and severity (*S*). The duration (*D*) of a drought event is represented by the length of the consecutive dry period, while the severity (*S*) quantifies the total magnitude of the dry periods, as depicted in Figure 3.

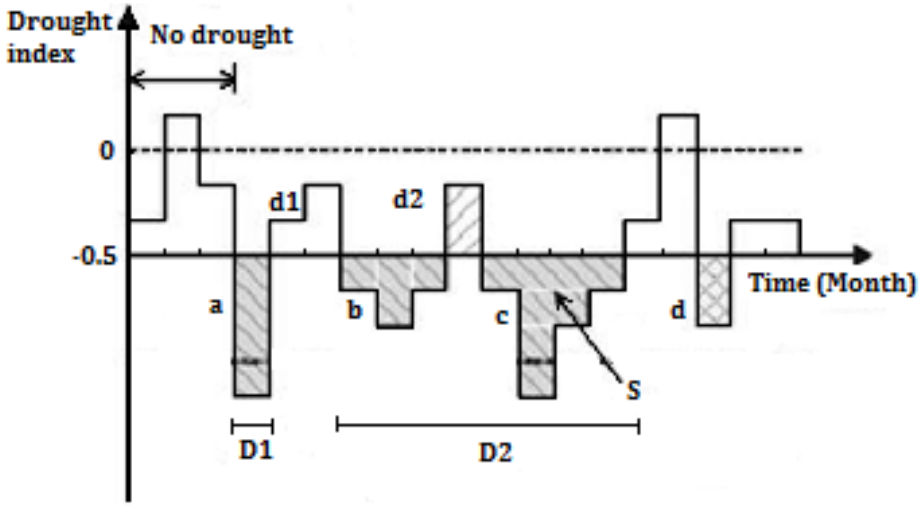

Figure 3. Schematic diagram illustrating the identification of drought events and their characteristics. D1 and D2 represent different duration of the drought. d1 and d2 represent the values of D1 and D2, respectively. *S* represents the drought severity. Shadows (such as a, b, c, d) represent the values of drought severity.

Figure 3 presents a graphical representation of two thresholds located at −0.5 and 0 on the *Y*-axis. When the monthly drought index (referred to as RDI or NJHDI) falls below −0.5, the corresponding month is classified as a drought month. If the drought index in the subsequent month exceeds 0, or if the drought indices in the following two months both fall within the range of −0.5 and 0, the duration of the drought (*D*) is denoted as D1, and D1 is equal to the value "a". Conversely, if the drought index in the second month falls within the range of −0.5 and 0, but then in the third month drops below −0.5, the duration of the drought *(D)* is referred to as D2, and D2 is calculated as the sum of "b", "d2", and "c". Drought severity (*S*) is defined as the absolute sum of the drought index values observed during a drought period.

3.5. Copula-Based Drought Risk-Assessment Model

Given the significance of drought duration (*D*) and drought severity (*S*) as fundamental characteristics of drought events, this study aimed to assess drought risk by analyzing the joint probability distribution of *D* and *S* within specified threshold ranges. Furthermore, to analyze drought risk across different time scales, drought events were further categorized into sub-seasonal drought and seasonal drought.

3.5.1. Definition of Sub-Seasonal Drought and Seasonal Drought

In accordance with the definition of drought event and its associated characteristics outlined in Section 3.4, the drought duration (*D*) represents the consecutive count of dry months within a given drought period. Conversely, the drought severity (*S*) is quantified

as the absolute sum of the drought index values observed throughout the entire duration of the drought, as demonstrated in Equation (2).

$$S = \left| \sum_{i=1}^{n} I_i \right| \quad (2)$$

where I is the drought index such as RDI and NJHDI. n is the number of dry months during a drought period.

Within the domain of a drought event, the duration of the drought is directly affected by the magnitude of n. In order to distinguish between short-duration and long-duration drought events, this study introduces two classifications based on the duration of the drought. If the drought duration (D) falls within a single season, specifically when n is less than or equal to three, the drought event is classified as a sub-seasonal drought. Conversely, if the drought duration (D) exceeds three months, the drought event is categorized as a seasonal drought.

According to the drought index classification illustrated in Table 1, it is established that a month is categorized as dry if the corresponding drought index value (I) is lower than or equal to -0.5. Additionally, based on Equation (2), it is established that the severity of the drought (S) during these dry months is greater than or equal to 0.5. In the case of a drought persisting for two or three months, the severity (S) increases to a minimum threshold of 1.0 or 1.5, respectively. Consequently, for a sub-seasonal drought (Figure 4a), the threshold for the severity (S) should be set equal to or higher than the minimum value among all drought severities (S) in Figure 4a, which is larger than or equal to 0.5. Similarly, for a seasonal drought (Figure 4b), where the drought duration (D) exceeds three months and the corresponding drought severity (S) is greater than or equal to 1.5, the threshold for S should also be set at least as high as the minimum value among all drought severity (S) in Figure 4b, which is larger than or equal to 1.5.

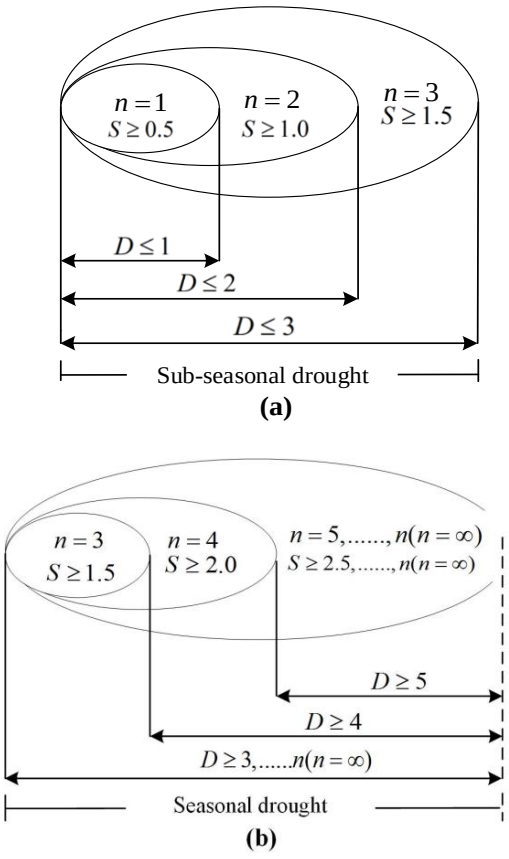

Figure 4. The definition of D and S of sub-seasonal drought (**a**) and seasonal drought (**b**).

In general, when a drought event is recognized as a sub-seasonal drought or a seasonal drought, the corresponding drought duration (D) and drought severity (S) should both satisfy the following conditions:

Sub-seasonal drought: $D \leq 3, S \geq 0.5$

Seasonal drought: $D \geq 3, S \geq 1.5$

3.5.2. Sub-Seasonal and Seasonal Drought Risk-Assessment Models

Copula function can be used to calculate the joint probability distribution of drought duration (D) and drought severity (S) that are both less than or equal to a given threshold, as shown below:

$$P(D \leq d, S \leq s) = C_\theta(F_D(d), F_S(s) \tag{3}$$

Based on Equation (3), the sub-seasonal and seasonal drought-risk probability models were established by mathematical deduction as follows:

Sub-seasonal drought risk-assessment model:

$$P(D \leq d, S \geq s) = F(d) - F(d, s) = F(d) - C_\theta(F(d_1), F(s)) \tag{4}$$

Seasonal drought risk-assessment model:

$$\begin{aligned} &P(D \geq d, S \geq s) = 1 - F(d) - F(s) + F(d, s) \\ &= 1 - F(d) - F(s) + C_\theta(F_D(d), F_S(s) \end{aligned} \tag{5}$$

where $F(d)$ and $F(s)$ are the marginal distribution functions of drought duration (D) and drought severity (S), respectively. $C_\theta(F_D(d), F_S(s)$ is the copula joint probability distribution.

In this study, the exponential distribution, lognormal distribution, and gamma distribution were employed to fit the marginal distribution of drought duration (D) and drought severity (S). Additionally, the Clayton, Frank, and Gumbel–Hougaard copulas were utilized to model the joint probability distribution. The selection of the most appropriate marginal distribution and copula functions was determined using the minimum Akaike information criterion (AIC) and bias. These criteria play a crucial role in ensuring the accuracy and reliability of the selected distributions and copulas.

4. Results and Discussion

4.1. Future Climate Changes in the YRB

This study employed the linear regression method to analyze the temporal trends of annual precipitation and temperature changes under two distinct scenarios from 2025 to 2060. The results are depicted in Figures 5 and 6. The analysis reveals noticeable disparities in the temporal trends of annual precipitation variation across the YRB regions under the different emission scenarios. Specifically, under the RCP4.5 scenario, there was a consistent increase in precipitation over time in each sub-zone, with a more pronounced escalation in the downstream compared to the upstream. However, under the RCP8.5 scenario, with the exception of the decreasing precipitation trend in the sub-zone E and sub-zone F over time, precipitation in other sub-zones demonstrated an increasing inclination temporally. Overall, the annual precipitation under the RCP8.5 scenario was marginally higher than that under the RCP4.5 scenario, although the difference was not statistically significant.

Consistent upward temporal trends in annual temperatures are evident across the YRB under the divergent emission scenarios. When comparing two scenarios, it was observed that sub-zone A and sub-zone C in the upstream exhibited slightly higher annual average temperatures under the RCP4.5 scenario compared to the RCP8.5 scenario, while the remaining four sub-zones demonstrated higher annual average temperatures under the RCP8.5 scenario relative to the RCP4.5 scenario. Furthermore, the rate of increase in annual average temperature under the RCP8.5 scenario was significantly higher than that under the RCP4.5 scenario.

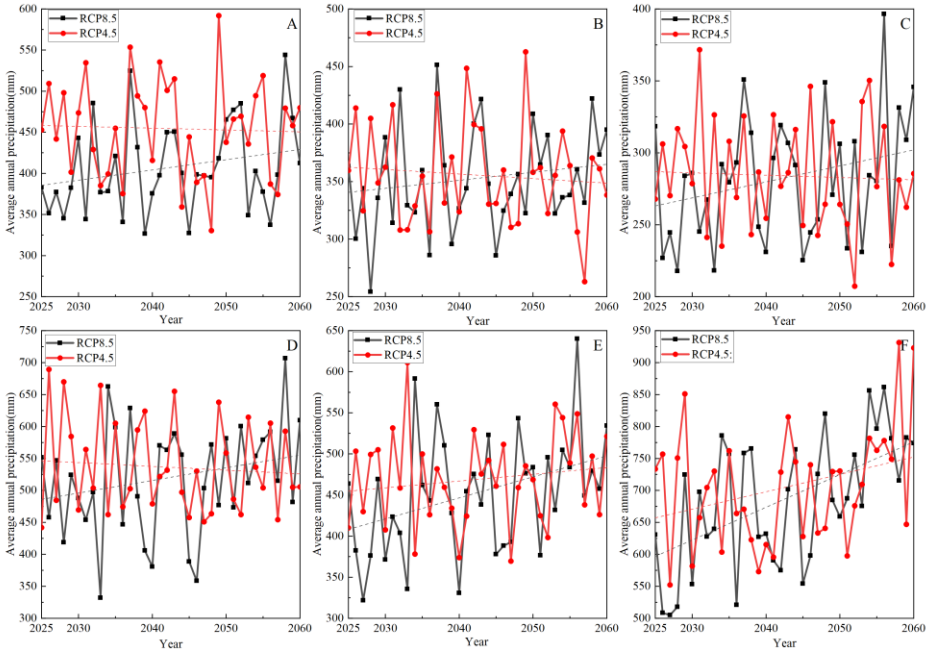

Figure 5. Annual precipitation change trends under two distinct scenarios from 2025 to 2060 in the YRB. The black and red dotted lines are change trend lines under RCP8.5 and RCP4.5 scenarios, respectively. (**A**) represents the semi-arid to semi-humid region. (**B**) represents the transitional zone between plateau and mid-temperate climates. (**C**) represents the arid to semi-arid region. (**D**) represents the semi-arid region. (**E**) represents the semi-arid to semi-humid zone. (**F**) represents the humid region.

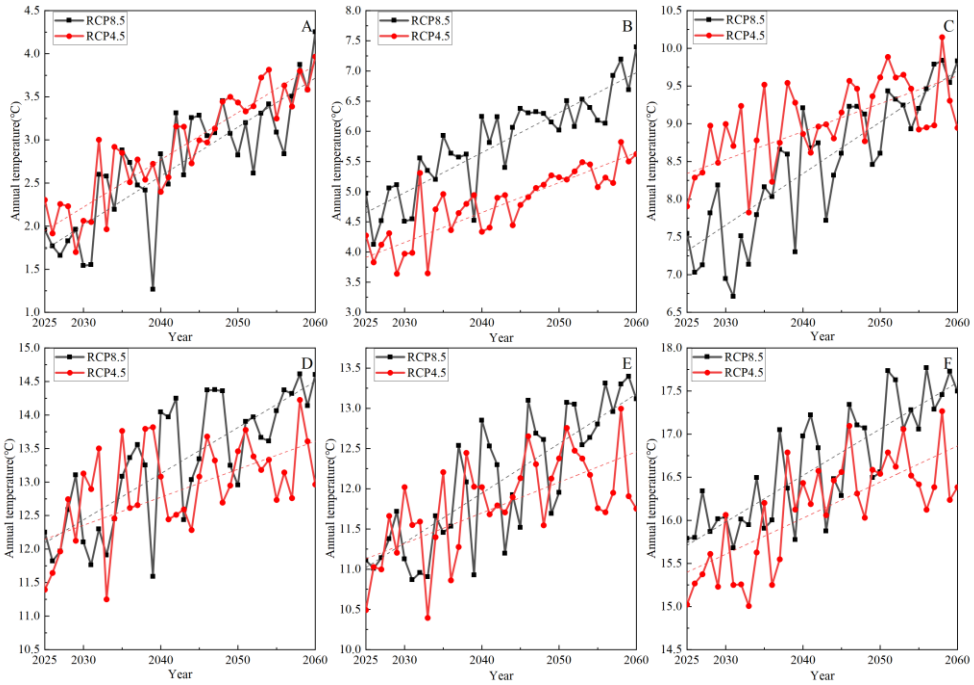

Figure 6. Annual temperature change trends under two distinct scenarios from 2025 to 2060 in the YRB. The black and red dotted lines are change trend lines under RCP8.5 and RCP4.5 scenarios, respectively. (**A**) represents the semi-arid to semi-humid region. (**B**) represents the transitional zone between plateau and mid-temperate climates. (**C**) represents the arid to semi-arid region. (**D**) represents the semi-arid region. (**E**) represents the semi-arid to semi-humid zone. (**F**) represents the humid region.

4.2. Future Land Use Changes in the YRB

The CA-Markov model, which utilizes equal intervals for simulating and predicting land-use patterns, employed the land-use patterns in 1990 and 2000 to predict land use in 2010, and the patterns in 2000 and 2010 to predict land use in 2020. To evaluate the accuracy of the CA-Markov model, *Kappa* coefficients were calculated for 2010 and 2020 by comparing the simulated land use with observed data using the crosstab module in IDRISI. The resulting Kappa coefficients for 2010 and 2020 are 0.8792 and 0.8850, respectively, both surpassing the threshold of 0.7. This indicates that the CA-Markov model is suitable and reliable for forecasting future land use changes in the YRB.

Based on the CA-Markov model, the historical land use pattern in 2020 serves as the starting point. It is combined with historical patterns in 2010, 2000, 1990, and 1980 to predict the land use patterns in 2030, 2040, 2050, and 2060 through 10, 20, 30, and 40 CA iterations, respectively. The results are illustrated in Figure 7, and quantification of land use area change characteristics during the period of 2020–2060 is presented in Table 2. Analysis of Figure 7 and Table 2 reveals a significant decline in grassland and cropland areas by approximately 14% in 2060 compared to 2020. Conversely, the areas of the remaining four land use types are projected to increase. Notably, the build-up area exhibits the most substantial expansion, estimated to be nearly 260% larger in 2060 than in 2020. This expansion can be attributed to rapid urban economic development, increased employment opportunities, and the migration of rural populations to urban areas, thereby accelerating the process of urbanization in the future.

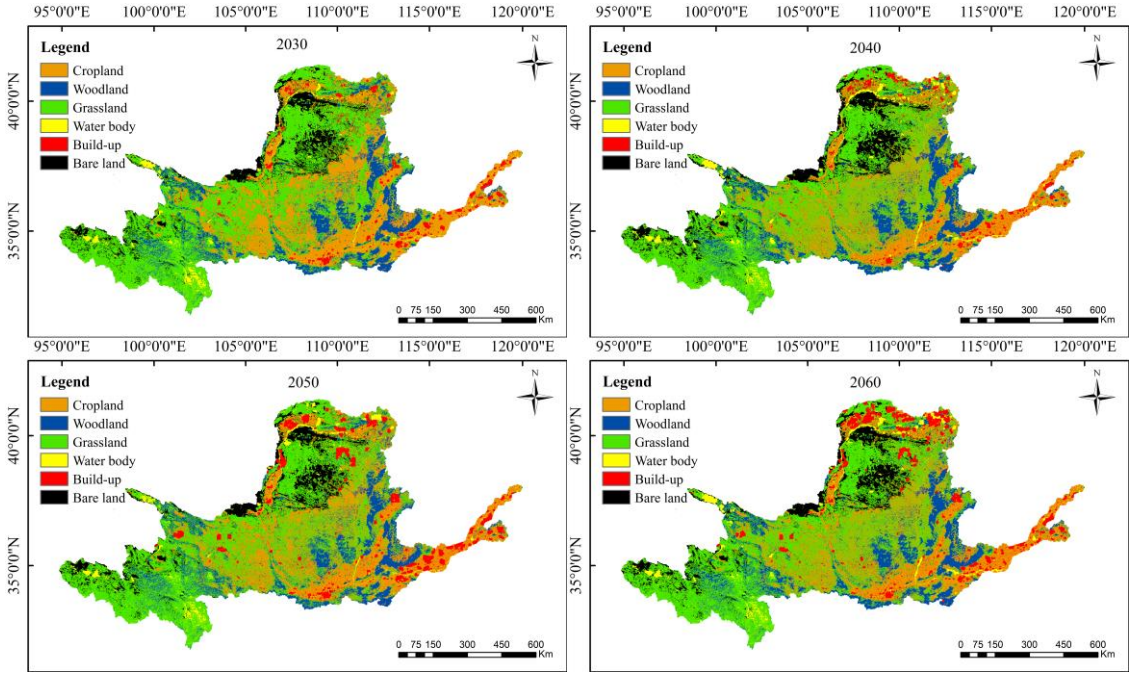

Figure 7. Prediction of land use patterns in 2030, 2040, 2050 and 2060 in the YRB.

Table 2. Area change characteristics of land use patterns during the period of 2020–2060 in the YRB.

Land Use Type	2020–2030		2030–2040		2040–2050		2050–2060		2020–2060	
	Area (km^2)	Ratio (%)	Area (km^2)	Ratio (%)	Area (km^2)	Ratio (%)	Area (km^2)	Ratio (%)	Area (km^2)	Ratio (%)
Cropland	−18,746	−8.34	6376	3.09	−20,754	−9.35	−11,240	−5.29	−216,504	−14.74
Woodland	5569	4.93	−7969	−6.72	5306	4.87	3675	3.32	3314	3.28
Grassland	−9261	−2.55	−6364	−1.80	−36,459	−9.52	−1445	−0.42	−206,952	−13.79
Water	5293	21.42	−2783	−9.28	8127	36.37	3070	11.28	5117	23.17
Build-up	3113	9.94	19,117	55.50	3587	63.16	4210	7.86	55,876	257.16
Bare land	14,033	20.60	−8378	−10.20	7962	11.79	1730	2.35	7962	11.79

4.3. SWAT Model Calibration and Validation

The YRB is initially divided into 381 sub-basins, with sizes ranging from 6 km^2 to 12,176 km^2, based on the Digital Elevation Model (DEM) and channel network. Subsequently, these sub-basins are further partitioned into 1850 hydrological response units (HRUs) using specific thresholds for dominant land use types, soil patterns, and slopes within each sub-basin. This division allows for enhanced simulation accuracy and a more comprehensive understanding of hydrological processes in the YRB. To calibrate and validate the SWAT model for the period of 1970–2015, streamflow observations from the main hydrological stations (see Figure 1) were employed. These stations, located within each subzone, were selected as they provide representation and data availability of the hydrological processes in the YRB.

In this study, a monthly time step was utilized for model runs. The spin-up period utilized the naturalized stream records from 1970 to establish initial conditions for the model experiment. Model calibration was then conducted using the naturalized stream records from 1971 to 1990, while model validation used data from 1991 to 2015. The calibration and validation results, evaluated using three metrics (i.e., R^2 and PBIAS), are presented in Table 3. Analysis of Table 3 reveals that the values of R^2 and in both calibration and validation periods exceeded 0.6 and 0.7, respectively. Furthermore, the absolute values of PBIAS remained within 25%. These results indicated that the SWAT model performs satisfactorily and is capable of reasonably simulating the hydrological processes influenced by climate and land use changes in the YRB.

Table 3. Calibration and validation results of the SWAT model measured by the three metrics.

Station	Calibration			Validation		
	Ens	**R^2**	**PBIAS (%)**	***Ens***	**R^2**	**PBIAS (%)**
Tangnaiai	0.83	0.85	−5.19	0.86	0.88	−10.38
Lanzhou	0.77	0.88	−8.77	0.80	0.90	−10.99
Toudaoguai	0.68	0.77	−16.12	0.71	0.79	−13.32
Huaxian	0.79	0.83	11.65	0.80	0.87	2.85
Huanyuankou	0.65	0.71	−20.64	0.64	0.75	−15.13

4.4. Meteorological Drought Risk Prediction

Selection of the appropriate marginal distribution and copula function of meteorological drought can be found in the Appendix A. Utilizing the meteorological drought risk assessment model, predictions were made for the risks of sub-seasonal and seasonal meteorological droughts in the future years of 2025–2060 across the six subzones of the YRB under the RCP 4.5 and RCP 8.5 scenarios. To provide a clearer representation of the spatial variation in meteorological drought risk, the spatial risk distributions of sub-seasonal and seasonal meteorological droughts under the two scenarios are illustrated in Figure 8.

Figure 8 reveals that the risks associated with seasonal meteorological droughts remained below 10% throughout the entire YRB under both scenarios. This suggests that the occurrence of seasonal meteorological droughts in the YRB is not expected to be significant in the next 35 years. However, sub-seasonal meteorological drought risks range from 40% to 50% within each subzone, indicating a potential increase in the frequency of sub-seasonal meteorological droughts in the YRB in the future. Additionally, the risk of sub-seasonal meteorological droughts is marginally higher in the upstream subzones (A, B, C) compared to the middle and lower reaches (D, E, F), with risks ranging from 46% to 50% in the upstream and 41% to 45% in the middle and lower reaches. When comparing the RCP 4.5 and RCP 8.5 scenarios, the risk of sub-seasonal meteorological droughts remained relatively stable, except for a 5% increase in the middle stream of zone E under the RCP 8.5 scenario.

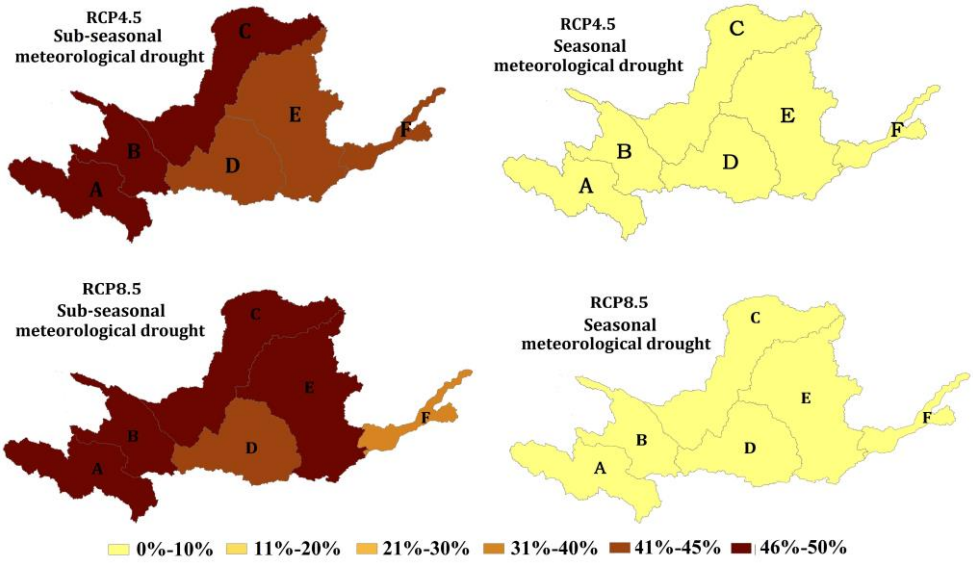

Figure 8. Spatial distributions of sub-seasonal and seasonal meteorological drought risks under two scenarios in the future years of 2025–2060 in the YRB. A represents the semi-arid to semi-humid region. B represents the transitional zone between plateau and mid-temperate climates. C represents the arid to semi-arid region. D represents the semi-arid region. E represents the semi-arid to semi-humid zone. F represents the humid region.

4.5. Hydrological Drought Risk Prediction

Selection of the appropriate marginal distribution and copula function of hydrological drought can be found in the Appendix A. Figure 9 illustrates the geographical distributions of sub-seasonal and seasonal hydrological drought risks under the RCP 4.5 and RCP 8.5 scenarios for the future years spanning 2025 to 2060 across the six subzones of the YRB. The findings from Figure 9 indicate that both sub-seasonal and seasonal hydrological drought risks exhibited significant spatial variability over the next 35 years.

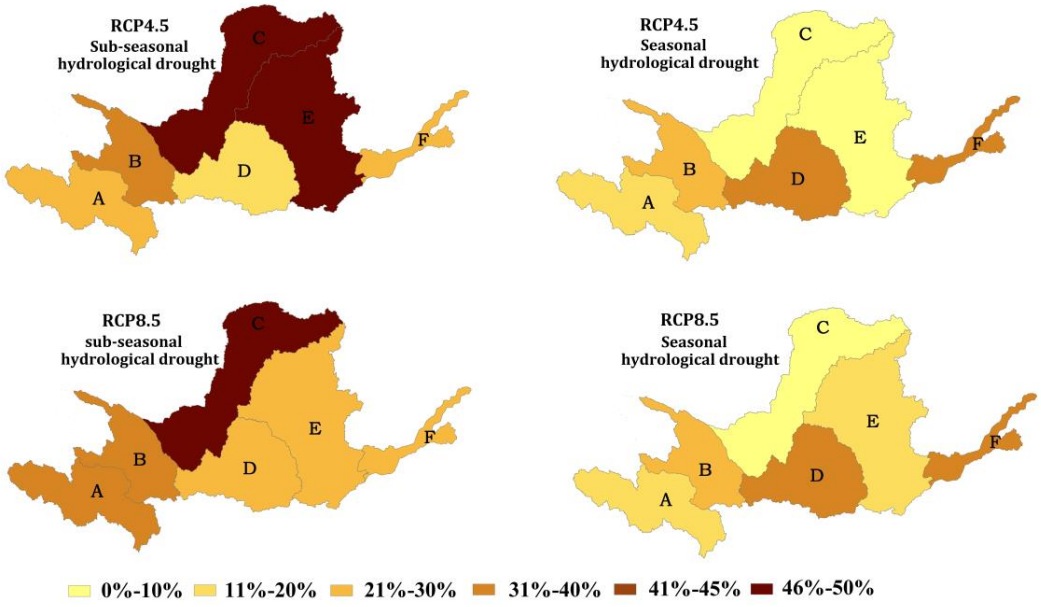

Figure 9. Spatial distributions of sub-seasonal and seasonal hydrological drought risks under two scenarios in the future years of 2025–2060 over the YRB. A represents the semi-arid to semi-humid region. B represents the transitional zone between plateau and mid-temperate climates. C represents the arid to semi-arid region. D represents the semi-arid region. E represents the semi-arid to semi-humid zone. F represents the humid region.

Under the RCP 4.5 scenario, sub-zones C and E, located in the Loess Plateau, are projected to face higher risks of sub-seasonal hydrological droughts, ranging from 45% to 50%. Conversely, these two subzones will experience lower risks of seasonal hydrological droughts, with probabilities of less than 10%. Sub-zones A and B will encounter risks ranging from 20% to 40% for sub-seasonal hydrological droughts, while their risks for seasonal hydrological droughts will decrease by 10% to 20%. Sub-zones D and F are expected to have risks of 10% to 30% for sub-seasonal hydrological droughts, while their risks for seasonal hydrological droughts will increase to 30% to 40%.

Under the RCP 8.5 scenario, sub-zone C will display the highest susceptibility to sub-seasonal hydrological droughts, with a probability of 45% to 50%. However, it will have the lowest probability of experiencing seasonal hydrological droughts, with a likelihood below 10%. Sub-zones A, B, and E will face higher risks of sub-seasonal hydrological droughts, ranging from 20% to 40%. However, these subzones will have lower risks of suffering from seasonal hydrological droughts, with probabilities within the range of 10% to 20%. Conversely, sub-zones D and F will be more prone to seasonal hydrological droughts, with probabilities ranging from 30% to 40%. However, their risks for sub-seasonal hydrological droughts will decrease to 20% to 30%.

In summary, the YRB is expected to be vulnerable to sub-seasonal hydrological drought, with risks ranging from 30% to 50%. Spatially, sub-zones C and E, both located in the Loess Plateau, exhibit the highest risks of experiencing sub-seasonal hydrological droughts, with probabilities ranging from 45% to 50%. It is important to note that the Loess Plateau is characterized by an extremely fragile ecological environment, making recovery from such drought events challenging.

4.6. Analysis of the Future Concerns Regarding Sub-Seasonal and Seasonal Droughts

It is challenging to assess whether the sub-seasonal and seasonal droughts, as defined in this study, will be of concern in the future for the YRB without understanding the extent to which future statistics deviate from historical data. Therefore, an analysis of the frequencies of sub-seasonal and seasonal droughts during the historical period from 1970 to 2015 is conducted to provide insights into their potential implications in the future. The findings of this analysis are presented in Figure 10.

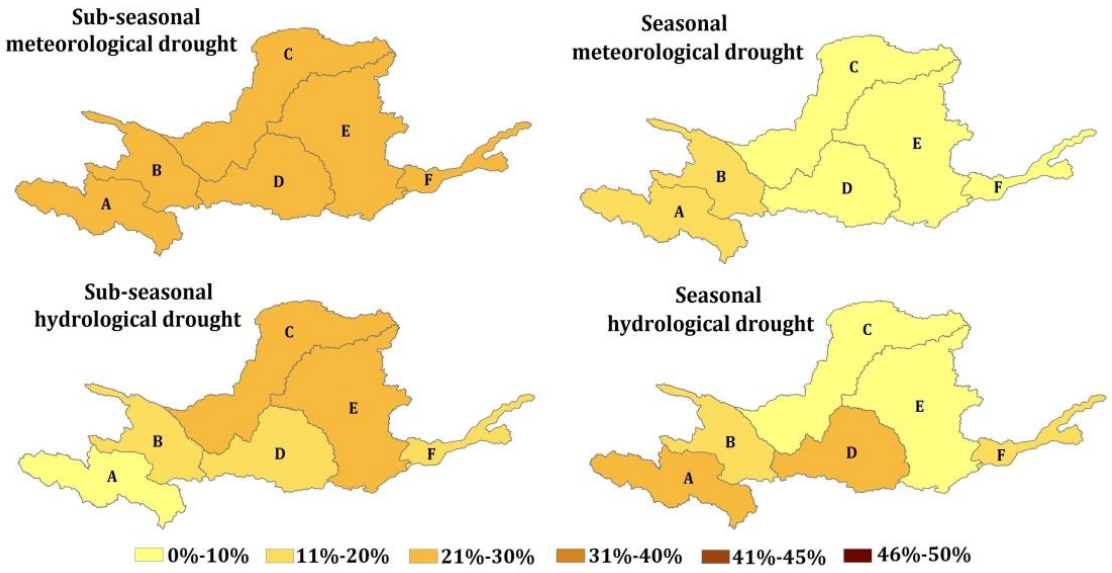

Figure 10. Spatial distributions of probabilities for sub-seasonal and seasonal meteorological and hydrological droughts during the historical period in the YRB. A represents the semi-arid to semi-humid region. B represents the transitional zone between plateau and mid-temperate climates. C represents the arid to semi-arid region. D represents the semi-arid region. E represents the semi-arid to semi-humid zone. F represents the humid region.

Figure 10 illustrates that the YRB has a higher probability of experiencing sub-seasonal droughts, both in terms of meteorology and hydrology, compared to seasonal droughts during the historical period. In terms of meteorological drought, the frequency of sub-seasonal drought ranged from 21% to 30% across the entire YRB, with little variation observed across different spatial zones. However, the frequency of seasonal drought in the upper reaches of the basin was slightly higher than in the lower reaches. Specifically, zones A and B exhibited drought frequencies of 11% to 20%, while the frequencies in the other four zones were less than 10%.

Regarding hydrological drought, there was significant spatial variation in both sub-seasonal and seasonal drought frequencies during the historical period. Sub-zones B and F had similar frequencies (11% to 20%) for both sub-seasonal and seasonal drought occurrences. Sub-zones C and E exhibited higher probabilities of experiencing sub-seasonal droughts, with frequencies ranging from 21% to 30%. However, these two sub-zones rarely experienced seasonal droughts, with frequencies below 10%. Conversely, sub-zones A and D were more prone to seasonal droughts than sub-seasonal droughts. The frequency of seasonal droughts in these sub-zones was 21% to 30%, while the frequency of sub-seasonal droughts decreased to 0% to 10% in sub-zone A and 11% to 20% in sub-zone D.

Compared to the historical period, the risks of sub-seasonal meteorological and hydrological droughts in the entire YRB are projected to significantly increase in the next 35 years under the RCP 4.5 and RCP 8.5 scenarios. The upstream areas (sub-zones A, B and C) will experience a 30–35% higher risk of sub-seasonal meteorological drought under both scenarios, with a range of 46–50%. In the middle and lower reaches (sub-zones D, E and F), the risk under the RCP 4.5 scenario will be 25–30% higher than historical levels, with a range of 41–45%. However, under the RCP 8.5 scenario, the risks of sub-seasonal meteorological droughts will vary across sub-zone D, and F, with increases of 25–30%, 30–35%, and 20%, respectively, compared to historical levels.

Regarding sub-seasonal hydrological droughts, sub-zone C will face the highest risk under both RCP 4.5 and RCP 8.5 scenarios in the future, with a 30–35% increase compared to historical levels. Similarly, under the RCP 4.5 scenario, sub-zone E will experience a 30–35% higher risk in the next 35 years. However, for the other four sub-zones, the risks of sub-seasonal hydrological droughts will not be a significant concern in the future, as the increases in risk will be below 10% compared to the historical period.

However, in comparison to the historical conditions, the likelihood of experiencing seasonal meteorological and hydrological droughts in the majority of the YRB will remain relatively unchanged in the next 35 years under the RCP 4.5 and RCP 8.5 scenarios. The risks associated with seasonal meteorological drought in the entire YRB under both scenarios are very low, with probabilities below 10%. However, it is important to monitor the downstream area of the YRB (sub-zone F) in the future, as the risk of seasonal hydrological drought in this region will be 20% higher than in the historical period.

In summary, the analysis indicated that the future risks of sub-seasonal meteorological and hydrological droughts in the YRB are a cause for concern. The upstream areas (sub-zones A, B and C) and the Loess Plateau (sub-zones C and E) are particularly vulnerable to these droughts, with projected risk increases of 30–35% compared to the historical period. While meteorological droughts in the entire YRB are not expected to be a significant concern in the future, the downstream area (zone F) should be closely monitored as the risk of seasonal hydrological droughts is projected to increase by 20%.

4.7. The Relationship between Meteorological- and Hydrological-Drought Risk Patterns

Furthermore, the analysis of Figures 8 and 9 revealed significant differences between meteorological and hydrological drought risk patterns. In both scenarios, the YRB is expected to experience a higher frequency of sub-seasonal meteorological drought compared to seasonal meteorological drought. This indicates that meteorological droughts are more likely to occur than hydrological droughts. However, the duration of hydrological drought is expected to be longer than that of meteorological drought. The increased frequency

of meteorological drought can be attributed to two factors. Firstly, mild meteorological droughts may not necessarily lead to hydrological droughts within a specific timeframe. Secondly, the short intervals between hydrological droughts make it easier to identify them as distinct drought events, resulting in a higher frequency of meteorological droughts. The shorter duration of meteorological drought in comparison to hydrological drought can be attributed to the relative ease of restoring the balance between precipitation and evaporation. When meteorological conditions change, an increase in precipitation or a decrease in evaporation can quickly alleviate meteorological drought. However, the recovery of surface water and groundwater resources may lag behind for longer periods of time. Consequently, even after meteorological droughts have been alleviated, surface water and groundwater may not replenish immediately. As a result, the duration of hydrological droughts surpasses that of meteorological droughts.

From a hydrological cycle perspective, there is a well-established connection between meteorological drought and hydrological drought. The equilibrium between precipitation and evaporation is easily disrupted by fluctuations in meteorological conditions, leading to the onset of meteorological drought. When meteorological drought persists, it triggers two key factors that contribute to hydrological drought. Firstly, prolonged meteorological droughts intensify surface water and groundwater evaporation, thereby depleting these resources. Secondly, this extended meteorological drought can cause the vadose zone to thicken and dry out, reducing surface water runoff and groundwater recharge. These two aspects play a crucial role in inducing hydrological drought, as a prolonged meteorological drought eventually results in the occurrence of hydrological drought. The duration of this phenomenon is influenced not only by climate factors but also by the characteristics of the underlying surfaces in the region. Different land use patterns can result in distinct mechanisms of runoff generation, which can either exacerbate or mitigate hydrological drought under the same climatic conditions. For instance, woodland and grassland possess higher water retention capacities in the soil, facilitating augmented recharge into groundwater. Consequently, when meteorological drought occurs, these land use patterns can alleviate the severity of hydrological drought compared to urbanized areas.

Based on the land use projections outlined in Section 4.2, future urban development, especially in the middle and downstream regions of the YRB, will undergo substantial expansion. This urban sprawl will have profound impacts on hydrological drought occurrence when meteorological drought episodes transpire. The intensified urbanization can hinder groundwater recharge due to impermeable underlying surfaces during periods of precipitation deficit.

This finding further elucidates the reasons behind the projected concerns of sub-seasonal hydrological drought in Zone C and Zone E, as well as seasonal hydrological drought in Zone F, as highlighted in Section 4.5. The considerable expansion of urban land in these zones exacerbates the challenges associated with hydrological drought, as the limited recharge of groundwater during meteorological droughts becomes even more difficult due to the impervious nature of the underlying surfaces.

5. Conclusions

This study utilized future climate projections from 2025–2060 under RCP 4.5 and RCP 8.5 scenarios, obtained from the BCC-CSM1-1 model data in the NASA Earth Exchange Global Daily Downscaled Projections (NEX-GDDP) dataset. The downscaled climate projections were then coupled with land-use-change modeling to estimate sub-seasonal and seasonal drought risks across the YRB over the next 35 years. Comparative and connectivity analyses were conducted to determine the significance of projected events and relationships between meteorological and hydrological drought hazards.

The findings indicate that sub-seasonal meteorological and hydrological droughts will pose significant issues in the YRB in the future. Specifically, greater attention should be paid to sub-seasonal meteorological drought risks in the upstream areas of the YRB (zones A, B, C), as these areas are projected to experience a 30–35% increase in risks compared to

historical levels. Similarly, increased focus on sub-seasonal hydrological drought is needed for the Loess Plateau (zones C, E), as risks in these areas are also projected to be 30–35% higher than historical periods. In contrast, the future impact of seasonal meteorological droughts in the YRB is predicted to be negligible, with risk levels below 10%. However, downstream YRB areas (zone F) should be alert to increasing hydrological drought risks, projected to rise 20% from historical conditions. The concerns about hydrological droughts in zones C, E, and F are primarily attributed to anticipated rapid urban expansion in the YRB's middle and downstream areas, which will likely exacerbate hydrological drought occurrence when meteorological droughts happen. In summary, sub-seasonal meteorological and hydrological drought risks are projected to significantly increase in most sub-basins of the YRB, highlighting the need for proactive adaptation and mitigation measures. The exceptions are seasonal meteorological droughts, which show minimal future risk escalation. However, it is important to note that urbanization remains a threat multiplier for hydrological droughts basin-wide when meteorological droughts occur.

This study represents a significant scientific effort to investigate and forecast the spatial distribution of sub-seasonal and seasonal meteorological and hydrological drought risks in the YRB. The results of this study provide an important foundation for decision support in addressing sub-seasonal and seasonal droughts through localized risk forecasts. Additionally, this study promotes the use of integrated methodologies that can be replicated in other climate-vulnerable regions to aid in adaptation and resilience efforts. By providing practical tools and methodological blueprints, this study contributes valuable insights to drought prediction and planning.

However, it is important to acknowledge the limitation of this study, which is the lack of incorporation of future water resource development and utilization in the prediction of hydrological drought risks. Factors such as reservoir storage, irrigation, industrial and domestic water consumption, and agricultural water use have not been accounted for in the modeling approach. The future scope of this work will aim to integrate water resource development and utilization projections, derived from socioeconomic scenarios, land-use-change modeling, and water planning forecasts. This would provide a more complete picture of the interacting natural and anthropogenic factors influencing hydrological drought risk out to the mid-21st century.

Author Contributions: Y.L.(Yunyun Li): investigation, formal analysis, and writing—original draft; Y.H.: conceptualization and methodology; J.F.: investigation and formal analysis; H.Z. and Y.L. (Yanchun Li): validation; X.W. and Q.D.: methodology and supervision. All authors have read and agreed to the published version of the manuscript.

Funding: This research was funded by the National Natural Science Foundation of China (Grant number 52009053), Natural Science Foundation of Mianyang Normal University (Grant number QD2020A06), and National Natural Science Foundation of China (Grant number 52209013, 52209008, 32101363).

Institutional Review Board Statement: Not applicable.

Informed Consent Statement: Not applicable.

Data Availability Statement: The datasets analyzed during the current study are available from the corresponding author on reasonable request due to privacy.

Conflicts of Interest: The authors declare no conflict of interest.

Appendix A

To further validate the accuracy of the Next-Generation Daily Downscaled Projections (NEX-GDDP) BCC-CSM1-1 model data predictions across the YRB, a total of 4296 spatially distributed grid point data were extracted and used to derive monthly average precipitation, maximum temperature, and minimum temperature for each subzone from 1970–2005. Figures A1–A3 present a comparison between these modeled sequences and observed station data. The monthly precipitation, maximum temperature, and minimum temperature modeled by BCC-CSM1-1 all show strong agreement with observed station values. Precipitation correlations exceed 0.7, while maximum and minimum temperature correlations surpass 0.9 across subzones. These high correlations indicate the BCC-CSM1-1 downscaled data accurately simulates the climate characteristics in the YRB. Consequently, this dataset can provide a robust foundation for projecting future drought evolution trends across the spatially diverse YRB.

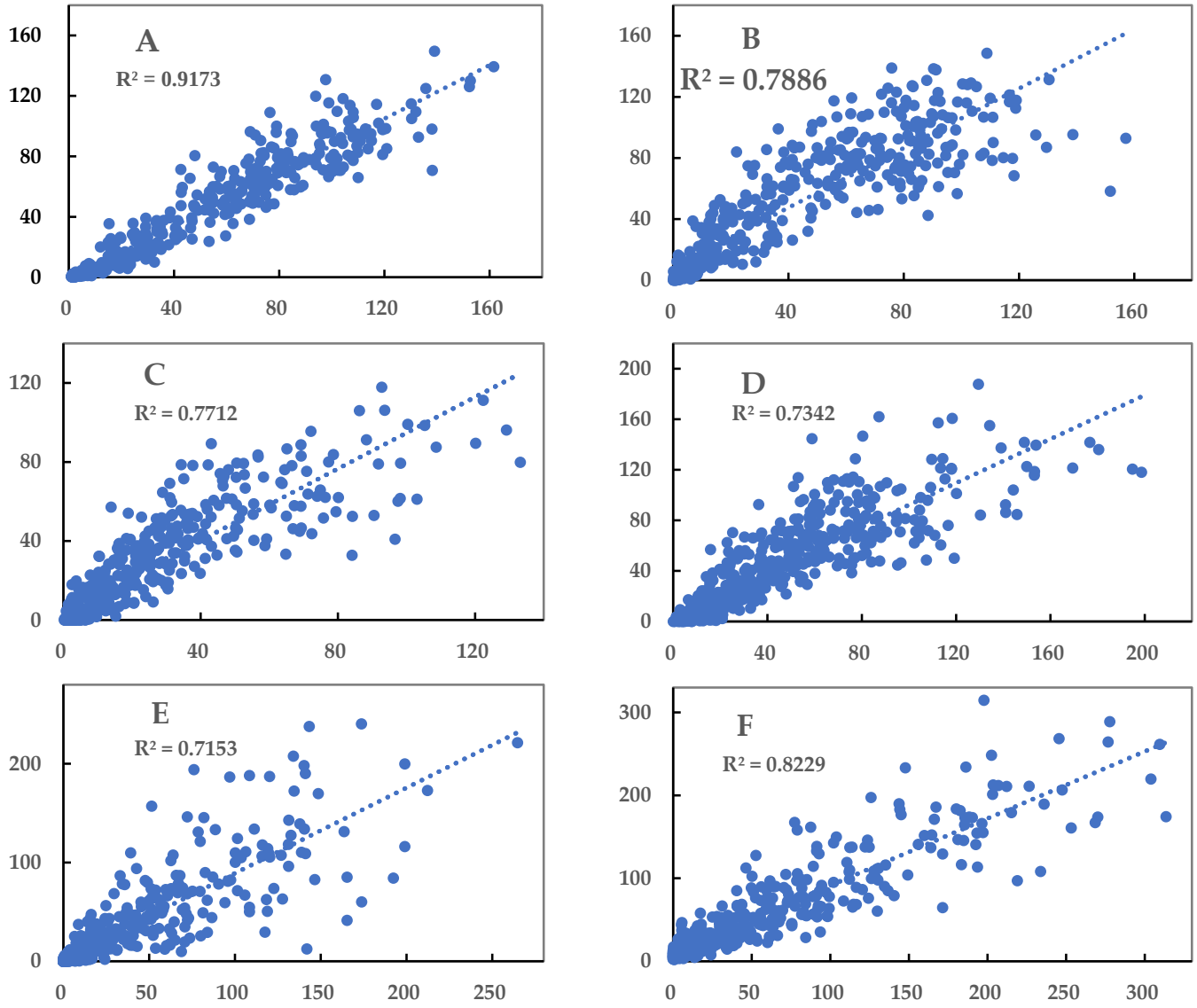

Figure A1. Comparative diagram of observed values and model forecast values of monthly precipitation in each subzones in 1970–2005 of the YRB. (**A**) represents the semi-arid to semi-humid region. (**B**) represents the transitional zone between plateau and mid-temperate climates. (**C**) represents the arid to semi-arid region. (**D**) represents the semi-arid region. (**E**) represents the semi-arid to semi-humid zone. (**F**) represents the humid region.

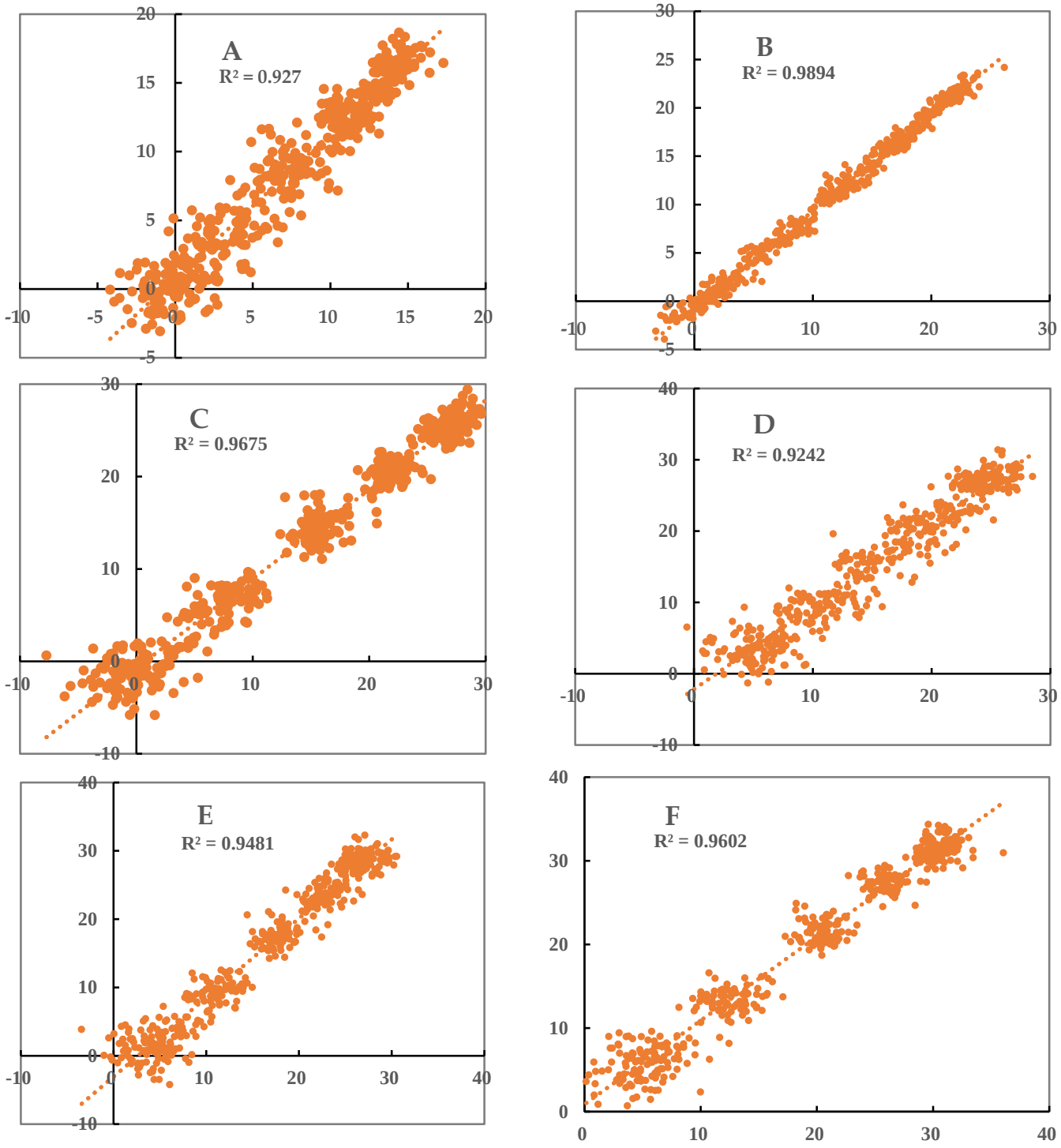

Figure A2. Comparative diagram of observed values and model forecast values of monthly maximum temperature in each subzones in 1970−2005 of the YRB. (**A**) represents the semi-arid to semi-humid region. (**B**) represents the transitional zone between plateau and mid-temperate climates. (**C**) represents the arid to semi-arid region. (**D**) represents the semi-arid region. (**E**) represents the semi-arid to semi-humid zone. (**F**) represents the humid region.

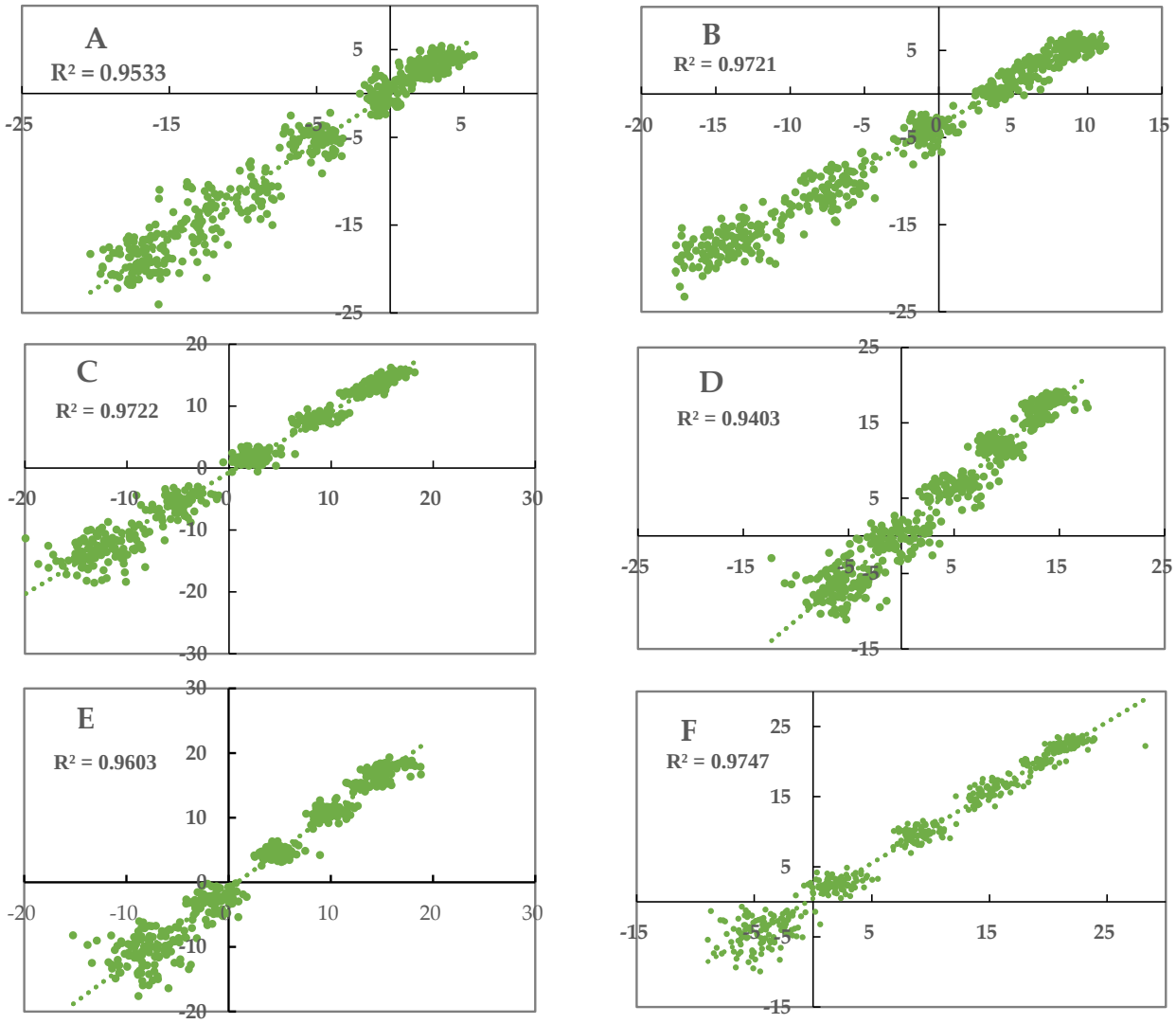

Figure A3. Comparative diagram of observed values and model forecast values of monthly minimum temperature in each subzones in 1970−2005 of the YRB. (**A**) represents the semi-arid to semi-humid region. (**B**) represents the transitional zone between plateau and mid-temperate climates. (**C**) represents the arid to semi-arid region. (**D**) represents the semi-arid region. (**E**) represents the semi-arid to semi-humid zone. (**F**) represents the humid region.

References

1. EM-DAT: Disasters in Numbers. 2012. Available online: www.emdat.be/ (accessed on 14 March 2013).
2. EEA. *Urban Adaptation to Climate Change in Europe: Challenges and Opportunities for Cities Together with Supportive National and European Policies*; Report No 2/2012; European Environment Agency: Copenhagen, Denmark, 2012.
3. Peterson, T.C.; Alexander, L.V.; Allen, M.R.; Anel, J.A.; Zhou, T.J. Explaining extreme events of 2012 from a climate perspective. *Bull. Am. Meteorol. Soc.* **2013**, *94*, S1–S74. [CrossRef]
4. Dutra, E.; Pozzi, W.; Wetterhall, F.; Giuseppe, F.D.; Magnusson, L.; Naumann, G.; Barbosa, P.; Vogt, J.; Pappenberger, F. Global meteorological drought—Part 2: Seasonal forecasts. *Hydrol. Earth Syst. Sci.* **2014**, *11*, 919–944. [CrossRef]
5. Seager, R.; Hoerling, M.; Schubert, S.; Wang, H.; Lyon, B.; Kumar, A.; Nakamura, J.; Henderson, N. Causes of the 2011–14 California Drought. *J. Clim.* **2015**, *28*, 6997–7024. [CrossRef]
6. Hao, Z.; Singh, V.P.; Xia, Y. Seasonal drought prediction: Advances, challenges, and future prospects. *Rev. Geophys.* **2018**, *56*, 108–141. [CrossRef]
7. Liu, Y.; Shan, F.Z.; Yue, H.; Wang, X.; Fan, Y.H. Global analysis of the correlation and propagation among meteorological, agricultural, surface water, and groundwater droughts. *J. Environ. Manag.* **2023**, *333*, 117460. [CrossRef]
8. Huang, S.Z.; Chang, J.X.; Leng, G.Y.; Huang, Q. Integrated index for drought assessment based on variable fuzzy set theory: A case study in the Yellow River Basin, China. *J. Hydrol.* **2015**, *527*, 608–618. [CrossRef]

9. Ma, M.; Ren, L.; Singh, V.P.; Fei, Y.; Lu, C.; Yang, X. Hydrologic model-based palmer indices for drought characterization in the yellow river basin, China. *Stoch. Environ. Res. Risk Assess.* **2016**, *30*, 1401–1420. [CrossRef]
10. Wang, F.; Wang, Z.M.; Yang, H.B.; Di, D.Y.; Zhao, Y.; Liang, Q.H.; Hussain, Z. Copula-Based Drought Analysis Using Standardized Precipitation Evapotranspiration Index: A Case Study in the Yellow River Basin, China. *Water* **2019**, *11*, 1298. [CrossRef]
11. Song, M.W.; Jiang, X.H.; Lei, Y.X.; Zhao, Y.R.; Cai, W.J. Spatial and temporal variation characteristics of extreme hydrometeorological events in the Yellow River Basin and their effects on vegetation. *Nat. Hazards* **2023**, *116*, 1863–1878. [CrossRef]
12. Zhu, Y.L.; Chang, J.X.; Huang, S.Z.; Huang, Q. Characteristics of integrated droughts based on a nonparametric standardized drought index in the Yellow River Basin, China. *Hydrol. Res.* **2016**, *47*, 454–467. [CrossRef]
13. Li, Y.Y.; Luo, L.F.; Chang, J.X.; Wang, Y.M.; Guo, A.J.; Fan, J.J.; Liu, Q. Hydrological drought evolution with a nonlinear joint index in regions with significant changes in underlying surface. *J. Hydrol.* **2020**, *585*, 124794. [CrossRef]
14. Wang, F.; Wang, Z.M.; Yang, H.B.; Di, D.Y.; Zhao, Y.; Liang, Q.H.; Hussain, Z. Comprehensive evaluation of hydrological drought and its relationships with meteorological drought in the Yellow River basin, China. *J. Hydrol.* **2020**, *584*, 124751. [CrossRef]
15. Ji, G.X.; Lai, Z.Z.; Yan, D.; Wu, L.Y.; Wang, Z. Spatiotemporal patterns of future meteorological drought in the Yellow River Basin based on SPEI under RCP scenarios. *Int. J. Clim. Change Strateg. Manag.* **2022**, *14*, 39–53. [CrossRef]
16. Wang, L.; Shu, Z.K.; Wang, G.Q.; Sun, Z.L.; Yan, H.F.; Bao, Z.X. Analysis of Future Meteorological Drought Changes in the Yellow River Basin under Climate Change. *Water* **2022**, *14*, 1896. [CrossRef]
17. Zhang, T.; Su, X.L.; Zhang, G.X.; Wu, H.J.; Liu, Y.H. Projections of the characteristics and probability of spatially concurrent hydrological drought in a cascade reservoirs area under CMIP6. *J. Hydrol.* **2022**, *613*, 128472. [CrossRef]
18. Li, Y.Y.; Chang, J.X.; Luo, L.F.; Wang, Y.M.; Guo, A.J.; Fan, J.J. Spatiotemporal impacts of land use land cover changes on hydrology from the mechanism perspective using swat model with time-varying parameters. *Hydrol. Res.* **2019**, *50*, 244–261. [CrossRef]
19. Wong, G.; Van Lanen, H.A.J.; Torfs, P.J.J.F. Probabilistic analysis of hydrological drought characteristics using meteorological drought. *Hydrol. Sci. J.-J. Des Sci. Hydrol.* **2013**, *58*, 253–270. [CrossRef]
20. Zhang, D.D.; Yan, D.H.; Lu, F.; Wang, Y.C.; Feng, J. Copula-based risk assessment of drought in Yunnan province, China. *Nat. Hazards* **2015**, *75*, 2199–2220. [CrossRef]
21. Yang, J.; Chang, J.X.; Wang, Y.M.; Li, Y.Y.; Hu, H.; Chen, Y.T.; Yao, J. Comprehensive drought characteristics analysis based on a nonlinear multivariate drought index. *J. Hydrol.* **2018**, *557*, 651–667. [CrossRef]
22. She, D.; Xia, J. Copulas-based drought characteristics analysis and risk assessment across the loess plateau of China. *Water Resour. Manag.* **2018**, *32*, 547–564. [CrossRef]
23. Ullah, H.; Akbar, M. Bivariate Drought Risk Assessment for Water Planning Using Copula Function in Balochistan. *J. Environ. Model. Assess.* **2023**, *28*, 447–464. [CrossRef]
24. Dai, M.; Huang, S.Z.; Huang, Q.; Leng, G.Y.; Guo, Y.; Wang, L.; Fang, W.; Li, P.; Zheng, X.D. Assessing agricultural drought risk and its dynamic evolution characteristics. *Agric. Gricultural Water Manag.* **2020**, *231*, 106003. [CrossRef]
25. Yu, J.; Kim, J.E.; Lee, J.H.; Kim, T.W. Development of a PCA-Based Vulnerability and Copula-Based Hazard Analysis for Assessing Regional Drought Risk. *Ksce J. Civ. Eng.* **2021**, *25*, 1901–1908.
26. Chang, J.X.; Li, Y.Y.; Wang, Y.M.; Yuan, M. Copula-based drought risk assessment combined with an integrated index in the Wei River Basin, China. *J. Hydrol.* **2016**, *540*, 824–834. [CrossRef]
27. Shaw, B.; Chithra, N.R. Copula-based multivariate analysis of hydro-meteorological drought. *Theor. Appl. Climatol.* **2023**, *153*, 475–493. [CrossRef]
28. Ali, J.; Syed, K.H.; Gabriel, H.F.; Saeed, F.; Ahmad, B.; Bukhari, S.A.A. Centennial heat wave projections over Pakistan using ensemble nex gddp data set. *Earth Syst. Environ.* **2018**, *2*, 437–454. [CrossRef]
29. Das, S.; Das, J.; Umamahesh, N.V. Identification of future meteorological drought hotspots over Indian region: A study based on NEX-GDDP data. *Int. J. Climatol.* **2021**, *41*, 5644–5662. [CrossRef]
30. Wu, Y.; Miao, C.; Duan, Q.; Shen, C.; Fan, X. Evaluation and projection of daily maximum and minimum temperatures over China using the high-resolution NEX-GDDP dataset. *Clim. Dyn.* **2020**, *55*, 2615–2629. [CrossRef]
31. Singh, S.; Jain, S.K.; Singh, P.K. Inter-comparisons and applicability of CMIP5 GCMs, RCMs and statistically downscaled NEX-GDDP based precipitation in India. *Sci. Total Environ.* **2019**, *697*, 134163. [CrossRef]
32. Li, Y.; Chen, Y.; Wang, F.; He, Y.; Li, Z. Evaluation and projection of snowfall changes in High Mountain Asia based on NASA's NEX-GDDP high-resolution daily downscaled dataset. *Environ. Res. Lett.* **2020**, *15*, 104040. [CrossRef]
33. Xiong, Y.; Xin, X.; Kou, X. Simulation and Projection of Near-Surface Wind Speeds in China by BCC-CSM Models. *J. Meteorol. Res.* **2019**, *33*, 149–158. [CrossRef]
34. Vicente-Serrano, S.; Schrier, G.; Beguería, S.; Azorin-Molina, C.; Lopez-Moreno, J. Contribution of precipitation and reference evapotranspiration to drought indices under different climates. *J. Hydrol.* **2015**, *526*, 42–54. [CrossRef]
35. Cammalleri, C.; Micale, F.; Vogt, J. A novel soil moisture-based drought severity index (DSI) combining water deficit magnitude and frequency. *Hydrol. Process.* **2016**, *30*, 289–301. [CrossRef]
36. Mckee, T.; Doesken, N.; Kleist, J. The Relationship of drought frequency and duration to time scales. In Proceedings of the Eighth Conference on Applied Climatology, Anaheim, CA, USA, 17–22 January 1993; American Meteorological Society: Boston, MA, USA, 1993; pp. 179–184.
37. Wang, H.; He, B.; Zhang, Y.; Huang, L.; Chen, Z.; Liu, J. Response of ecosystem productivity to dry/wet conditions indicated by different drought indices. *Sci. Total Environ.* **2018**, *612*, 347–357. [CrossRef]

38. Khan, M.I.; Dong, L.; Qiang, F.; Faiz, M.A. Detecting the persistence of drying trends under changing climate conditions using four meteorological drought indices. *Meteorol. Appl.* **2018**, *13*, 184–194. [CrossRef]
39. Chen, H.; Sun, J. Changes in drought characteristics over China using the standardized precipitation evapotranspiration index. *J. Clim.* **2015**, *28*, 5430–5447. [CrossRef]
40. Zarch, M.A.A.; Sivakumar, B.; Sharma, A. Droughts in a warming climate: A global assessment of standardized precipitation index (SPI) and reconnaissance drought index (RDI). *J. Hydrol.* **2015**, *526*, 183–195. [CrossRef]
41. Tsakiris, G.; Vangelis, H. Establishing a drought index incorporating evapotranspiration. *Eur. Water* **2005**, *9*, 3–11.
42. Hoekema, D.J.; Sridhar, V. Relating climatic attributes and water resources allocation: A study using surface water supply and soil moisture indices in the snake river basin, Idaho. *Water Resour. Res.* **2011**, *47*, 209–216. [CrossRef]
43. Palmer, W.C. *Meteorological Drought*; Research Paper No. 45; US Weather Bureau: Washington, DC, USA, 1965; p. 58.
44. Wang, D.; Hejazi, M.; Cai, X.; Valocchi, A. Climate change impact on meteorological, agricultural, and hydrological drought in central Illinois. *Water Resour. Res.* **2011**, *47*, W09527. [CrossRef]
45. Svensson, C.; Hannaford, J.; Prosdocimi, I. Statistical distributions for monthly aggregations of precipitation and streamflow in drought indicator applications. *Water Resour. Res.* **2017**, *53*, 999–1018. [CrossRef]
46. Shahid, S.; Hazarika, M.K. Groundwater Drought in the Northwestern Districts of Bangladesh. *Water Resour. Manag.* **2010**, *24*, 1989–2006. [CrossRef]
47. Li, B.; Rodell, M. Evaluation of a model-based groundwater drought indicator in the conterminous U.S. *J. Hydrol.* **2015**, *526*, 78–88. [CrossRef]
48. Ottosen, C.B.; Ronde, V.; Trapp, S.; Bjerg, P.L.; Broholm, M.M. Phytoscreening for Vinyl Chloride in Groundwater Discharging to a Stream. *Ground Water Monit. Remediat.* **2018**, *38*, 66–74. [CrossRef]
49. Berberoğlu, S.; Akın, A.; Clarke, K.C. Cellular automata modeling approaches to forecast urban growth for adana, Turkey: A comparative approach. *Landsc. Urban Plan.* **2016**, *153*, 11–27. [CrossRef]
50. Wangyel, W.; Lamchin, M.; Woo-Kyun, L. Land use and land cover change detection and prediction in Bhutan's high altitude city of Thimphu, using cellular automata and Markov chain. *Environ. Chall.* **2021**, *2*, 100017. [CrossRef]
51. Weng, Q. Land use change analysis in the Zhujiang Delta of China using satellite remote sensing, GIS and stochastic modelling. *J. Environ. Manag.* **2002**, *64*, 273–284. [CrossRef]
52. Guan, D.; Li, H.; Inohae, T.; Su, W.; Nagaie, T.; Hokao, K. Modeling urban land use change by the integration of cellular automaton and Markov model. *Ecol. Model.* **2011**, *222*, 3761–3772. [CrossRef]
53. Fuglsang, M.; Münier, B.; Hansen, H.S. Modelling land-use effects of future urbanization using cellular automata: An eastern Danish case. *Environ. Model. Softw.* **2013**, *50*, 1–11. [CrossRef]
54. Halmy, M.W.A.; Gessler, P.E.; Hicke, J.A.; Salem, B.B. Land use/land cover change detection and prediction in the north-western coastal desert of Egypt using Markov-Ca. *Appl. Geogr.* **2015**, *63*, 101–112. [CrossRef]
55. Gong, W.F.; Yuan, L.; Fan, W.Y.; Stott, P. Analysis and simulation of land use spatial pattern in Harbin prefecture based on trajectories and cellular automata-Markov modelling. *Int. J. Appl. Earth Obs. Geoinf.* **2015**, *34*, 207–216. [CrossRef]
56. Ghosh, P.; Mukhopadhyay, A.; Chanda, A.; Mondal, P.; Akhand, A.; Mukherjee, S. Application of Cellular automata and Markov-chain model in geospatial environmental modeling- A review. *Remote Sens. Appl. Soc. Environ.* **2017**, *5*, 64–77. [CrossRef]
57. Zhang, X.R.; Zhou, J.; Song, W. Simulating Urban Sprawl in China Based on the Artificial Neural Network-Cellular Automata-Markov Model. *Sustainability* **2020**, *12*, 4341. [CrossRef]
58. Okba, W.; Samir, B.; Moncef, S.M. Modelling and Assessing the Spatiotemporal Changes to Future Land Use Change Scenarios Using Remote Sensing and CA-Markov Model in the Mellegue Catchment. *J. Indian Soc. Remote Sens.* **2023**, *51*, 9–29.
59. Usman, M.; Ndehedehe, C.E.; Farah, H.; Ahmad, B.; Wong, Y.J.; Adeyeri, O.E. Application of a Conceptual Hydrological Model for Streamflow Prediction Using Multi-Source Precipitation Products in a Semi-Arid River Basin. *Water* **2022**, *14*, 1260. [CrossRef]
60. Maneechot, L.; Wong, Y.J.; Try, S.; Shimizu, Y.; Bharambe, K.P.; Hanittinan, P.; Ram-Indra, T.; Usman, M. Evaluating the necessity of post-processing techniques on d4PDF data for extreme climate assessment. *Envionmental Sci. Pollut. Res.* **2023**, *30*, 102531–102546. [CrossRef]
61. Nash, J.E.; Sutcliffe, J.V. River flow forecasting through conceptual models part I: A discussion of principles. *J. Hydrol.* **1970**, *10*, 282–290. [CrossRef]
62. Gupta, H.V.; Sorooshian, S.; Yapo, P.O. Status of Automatic Calibration for Hydrologic Models: Comparison with Multilevel Expert Calibration. *J. Hydrol. Eng.* **1999**, *4*, 135–143. [CrossRef]
63. Moriasi, D.N.; Arnold, J.G.; Liew, M.W.V.; Bingner, R.L.; Harmel, R.D.; Veith, T.L. Model evaluation guidelines for systematic quantification of accuracy in watershed simulations. *Trans. ASABE* **2007**, *50*, 885–900. [CrossRef]
64. Yevjevich, V.M. An Objective Approach to Definitions and Investigations of Continental Hydrologic Droughts. Hydrologic Paper No. 23. Bachelor's Thesis, Colorado State University, Fort Collins, CO, USA, 1967.